

Curved-Crease Origami for Morphing Metamaterials

Asma Karami¹, Adam Reddy¹, and Hussein Nassar^{1*}

Department of Mechanical and Aerospace Engineering, University of Missouri, Columbia, Missouri 65211, USA



(Received 10 April 2023; revised 24 September 2023; accepted 2 February 2024; published 7 March 2024)

We find a closed-form expression for the Poisson’s coefficient of curved-crease variants of the “Miura ori” origami tessellation. This is done by explicitly constructing a continuous one-parameter family of isometric piecewise-smooth surfaces that describes the action of folding out of a reference state. The response of the tessellations in bending is investigated as well: using a numerical convergence scheme, the effective normal curvatures under infinitesimal bending are found to occur in a ratio equal and opposite to the Poisson’s coefficient. These results are the first of their kind and, by their simplicity, should provide a fruitful benchmark for the design and modeling of curved-crease origami and compliant shell mechanisms. The developed methods are used to design a curved-crease 3D morphing solid with a tunable self-locked state.

DOI: [10.1103/PhysRevLett.132.108201](https://doi.org/10.1103/PhysRevLett.132.108201)

The properties of architected materials and metamaterials are just as much, if not more, a product of geometry and spatial layout as they are of the properties of the raw materials that they are made of. Here is a striking example from the classical theory of composites [1]: the effective Young’s modulus of an isotropic porous plate does not depend on the Poisson’s coefficient of the raw material and instead depends only on the spatial distribution of the pores [2]. Moreover, for highly porous plates, the effective Poisson’s coefficient is a pure product of geometry and is completely independent of the raw material [3].

Origami tessellations, as well as other architected materials composed of structural elements including bars and plates connected at joints, provide more recent examples where the Poisson’s coefficient is a purely geometric construct [4,5]. Such structures are near mechanisms and possess a soft deformation mode whose effective Cauchy-Green tensor \mathbf{I} defines the Poisson’s coefficient

$$\nu \equiv -\frac{dI_{22}/I_{22}}{dI_{11}/I_{11}}. \quad (1)$$

Typically, the soft deformation mode engages rotations at the joints and moves the structural elements as rigid bodies. This makes the computation of ν particularly straightforward, however algebraically complex it may be [6]. That said, there are highly compliant structures that cannot be treated in the same fashion, namely, as linkages, for their soft deformation modes necessarily involve the bending of the structural elements [7]. Examples include inextensible elastic curves and surfaces. For curved-crease origami [8], the difficulty is compound: On the one hand, the presence of curved folds couples folding angles to bending in the facets. On the other hand, the inextensible bending within facets still has to be compatible at the curved-crease lines.

Rigorous results in the field of curved-crease origami are relatively recent, even though a characterization of developable surfaces has been known since Euler. Recall that a developable surface is a smooth surface that is locally isometric to a plane; i.e., it is a surface assembled from planar pieces that are bent without stretching or creasing. Euler showed that developable surfaces are ruled: they are composed of straight segments of finite lengths. Furthermore, the ruling is torsal: the tangent plane maintains tangency along each rule segment [9]. What was lacking, and is currently actively researched, is an understanding of how the rule segments of different developable facets can fit together along crease lines and still produce a surface that is locally isometric to a plane. Demaine, Demaine and collaborators championed efforts in this area building on previous work by Huffman [10,11]. They were able to design, and prove the (mathematical) existence of, multiple curved-crease origami sculptures based on an understanding of which distributions of rule segments are compatible with which curved-crease lines [12–14]. Discretizations, guided by similar considerations, led to fruitful form-finding numerical tools [15–18]. Some semi-analytical asymptotic tools are also available for patterns composed of thin facets (or ribbons) [19,20]; see also [21].

In this Letter, a different approach is proposed. Rather than working facet by facet, a global isometry (by immersion) between the planar and folded state is directly constructed. The isometry is in fact one instance of a continuous one-parameter family of isometries for which closed-form expressions are provided. In particular, this allows one to compute the Poisson’s coefficient ν of a curved-crease origami tessellation via simple integration. Evidently, such methods are not universal but are applicable for a class of tessellations that, however restricted, is ubiquitous in engineering applications,

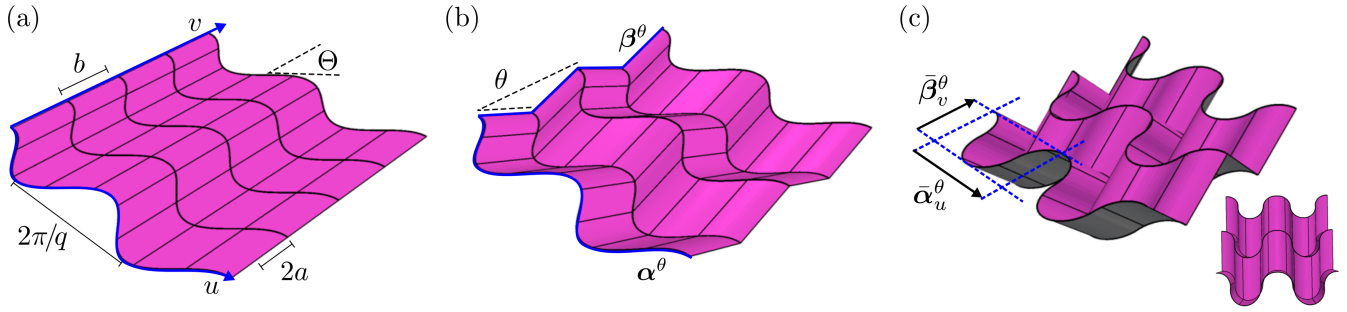


FIG. 1. Curved-crease variant of the Miura ori and the used notations. (a) Crease pattern in a flat reference configuration. Some ruling segments are revealed to improve visibility; the thicker curved lines are crease lines. (b) Partially folded state. (c) Fully folded state: $\theta = \Theta$. Inset: axial view that better shows the (locally) flat-folded ruling segments. The values used are $a = q = 1$, $\Theta = \pi/4$, and $b = 3$.

including curved-crease foldcores used in sandwich panels [22–24]. To present the approach, a curved-crease variant of the Miura ori is adopted as an archetypical example first. Generalizations to other patterns and applications to the design of curved-crease 3D compliant mechanisms follow.

Thus, let $\alpha: u \mapsto (u, a \sin(qu), 0)$ describe a sinusoidal curved crease of parameters ($a > 0, q > 0$), and let $\beta: v \mapsto (0, v, 0)$ describe a straight line. Consider the parametrization of the plane $\mathbf{x}: (u, v) \mapsto \alpha(u) + \beta(v)$ illustrated in Fig. 1(a). The purpose is to determine a one-parameter family of parametrized surfaces $\theta \mapsto \mathbf{x}^\theta$ that are isometric to \mathbf{x} . These surfaces must be piecewise smooth with jumps in the tangent plane located at a series of crease lines $\{v = mb\}$, with m an integer and b being a uniform spacing between two consecutive crease lines. The idea is to construct \mathbf{x}^θ as a “surface of translation,” i.e., in the form $\mathbf{x}^\theta: (u, v) \mapsto \alpha^\theta(u) + \beta^\theta(v)$, where the curves α^θ and β^θ are deduced from the originals α and β by maintaining the isometric character of the deformation, that is, such that

$$\begin{aligned} \langle \alpha_u^\theta(u), \alpha_u^\theta(u) \rangle &= \langle \alpha_u(u), \alpha_u(u) \rangle = 1 + a^2 q^2 \cos^2(qu), \\ \langle \beta_v^\theta(v), \beta_v^\theta(v) \rangle &= \langle \beta_v(v), \beta_v(v) \rangle = 1, \\ \langle \alpha_u^\theta(u), \beta_v^\theta(v) \rangle &= \langle \alpha_u(u), \beta_v(v) \rangle = aq \cos(qu), \end{aligned} \quad (2)$$

where the subscripts stand for derivatives. Hereafter, it will prove convenient to build α^θ and β^θ from their respective tangent vectors α_u^θ and β_v^θ by integration according to

$$\alpha^\theta(u) = \int_0^u \alpha_u^\theta(\xi) d\xi, \quad \beta^\theta(v) = \int_0^v \beta_v^\theta(\zeta) d\zeta. \quad (3)$$

Now intuition and experiment suggest β^θ be a “zigzag” of a tangent vector β_v^θ defined piecewise by

$$\beta_v^\theta(v) = \begin{cases} (0, \cos \theta, \sin \theta) & \text{for } 0 \leq v < b, \\ (0, \cos \theta, -\sin \theta) & \text{for } b \leq v < 2b, \end{cases} \quad (4)$$

and so on, by alternating signs. Then, let

$$\alpha_u^\theta(u) = \left(\sqrt{1 - a^2 q^2 \cos^2(qu) \tan^2 \theta}, aq \frac{\cos(qu)}{\cos \theta}, 0 \right) \quad (5)$$

so as to fulfill the requirement of \mathbf{x}^θ being isometric to \mathbf{x} , namely, Eq. (2). Furthermore, $\mathbf{x}^{\theta=0} = \mathbf{x}$. Accordingly, $\theta \mapsto \mathbf{x}^\theta$ parametrizes a continuous isometric deformation out of the planar state \mathbf{x} ; the family is illustrated in Fig. 1. The deformation parameter θ is the acute angle between the zigzag segments and the plane $\{z = 0\}$. That angle cannot be arbitrarily large and is bound by a value that corresponds to a maximally folded state. Indeed, \mathbf{x}^θ is well defined if, for all u ,

$$1 - a^2 q^2 \cos^2(qu) \tan^2 \theta \geq 0, \quad (6)$$

i.e., if

$$|\theta| \leq \frac{\pi}{2} - \arctan(aq) \equiv \Theta. \quad (7)$$

In other words, angle θ must remain smaller than the smallest angle that the curved crease α makes with the ruling $\{x = cst\}$, namely, Θ . As θ reaches its upper bound Θ , the triad composed of the tangents to the curved crease and to the two sides of the zigzag folds flat at $u = \pi m/q$ for any integer m [Fig. 1(c)].

It is noteworthy that the folded surfaces \mathbf{x}^θ are periodic with a unit cell $[0, 2\pi/q] \times [0, 2b]$, the same as the original crease pattern. Even though all of these surfaces are mutually isometric, it is possible to define an effective stretch based on the span of the image of the unit cell. Hence, let \mathbf{I}^θ be the effective metric of \mathbf{x}^θ given by

$$I_{11}^\theta = \langle \bar{\alpha}_u^\theta, \bar{\alpha}_u^\theta \rangle, \quad I_{22}^\theta = \langle \bar{\beta}_v^\theta, \bar{\beta}_v^\theta \rangle, \quad I_{12}^\theta = \langle \bar{\alpha}_u^\theta, \bar{\beta}_v^\theta \rangle, \quad (8)$$

where $\bar{\alpha}_u^\theta \equiv (q/2\pi) \int_0^{2\pi/q} \alpha_u^\theta du$ and $\bar{\beta}_v^\theta \equiv (1/2b) \int_0^{2b} \beta_v^\theta dv$. It is easy to verify that

$$I_{11}^\theta = \frac{4}{\pi^2} E^2(\mu), \quad I_{22}^\theta = \cos^2 \theta, \quad I_{12}^\theta = 0, \quad (9)$$

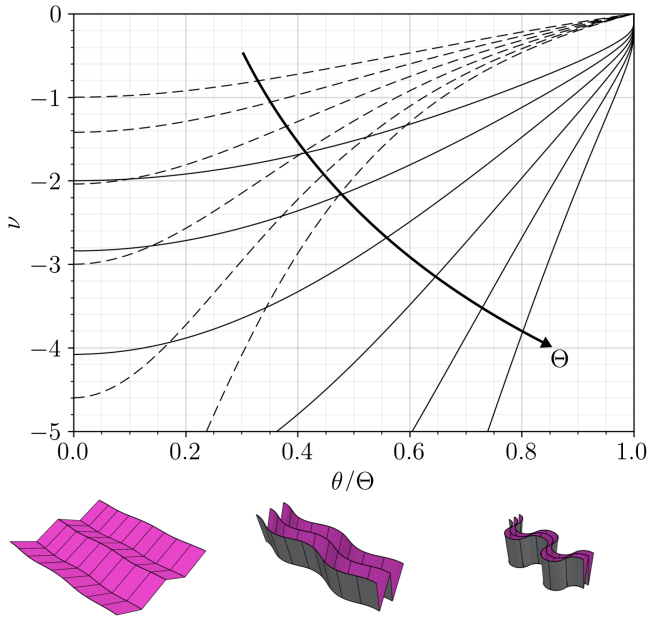


FIG. 2. Poisson's coefficient. Top panel: variations of the Poisson's coefficient vs the relative folding angle for both the original [6] Miura ori (dashed lines) and curved-crease variant (solid lines) with equal unit cell dimensions and maximum fold angle Θ ; angle Θ is sampled every 5° from 45° to 70° and increases with the arrow. Bottom sketches: folded states for an extreme value of $\Theta \sim \pi/2$; note how the motion proceeds in one direction, then in another.

where $\mathbb{E}(\mu)$ is the complete elliptic integral of the second kind evaluated at $\mu = a^2 q^2 \tan^2 \theta = \tan^2 \theta / \tan^2 \Theta$. In particular, at $\theta = 0$, $\mathbf{I}^{\theta=0} = \mathbf{I}$ is the identity. In conclusion of this section, letting $\mathbb{K}(\mu)$ be the complete elliptic integral of the first kind, the Poisson's coefficient is

$$\nu(\theta) \equiv -\frac{j_{22}^\theta / I_{22}^\theta}{j_{11}^\theta / I_{11}^\theta} = \frac{\tan^2 \theta}{1 + \tan^2 \theta} \frac{\mathbb{E}(\mu) - \mathbb{K}(\mu)}{\mathbb{E}(\mu)} \quad (10)$$

and is negative. The variations of the Poisson's coefficient of curved-crease variants of the Miura ori are illustrated in Fig. 2 (top panel). It is seen that the curved creases increase the Poisson's coefficient, in absolute value, by a factor of 2 for comparable maximum angles Θ and folding fractions θ/Θ . Note that for larger Θ , the Poisson's coefficient attains more extreme values because the foldings of the two curves α and β become increasingly decorrelated (Fig. 2, bottom sketches). It is important to stress that it is not clear whether or not the isometric deformation found is unique, and therefore whether it will occur as a mechanical response. That being said, finite element simulations carried over thin elastic shells suggest that the proposed isometric deformation indeed dominates the mechanical response, at least under periodic boundary conditions that are suitable for the extraction of effective properties; see Ref. [25].

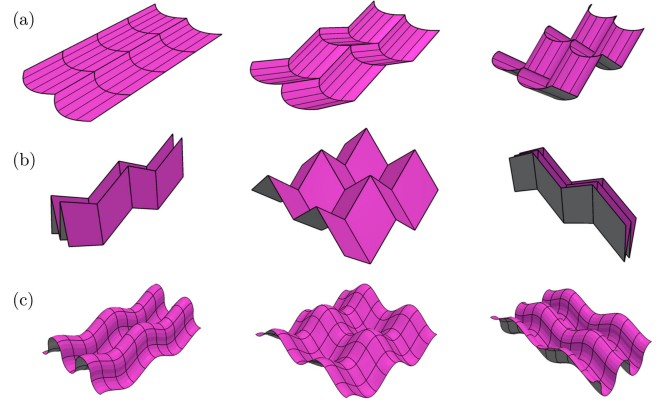


FIG. 3. Isometric deformations of surfaces of translation. (a) Surface with both straight and curved creases. (b) Non-developable surface with straight creases known as the eggbox pattern. (c) Creaseless smooth variant of (b).

The above formulas can be generalized in a straightforward fashion to curved creases $\alpha: u \mapsto (u, f(u), 0)$ with arbitrary profile f , be it smooth or piecewise smooth, as long as $|f'| < \infty$. In [26], Lee *et al.* investigated folded states where f described an elastica curve, but neither the folding motion \mathbf{x}^θ nor the Poisson's coefficient ν were provided. Closer to the foregoing investigations is the work of Mundilova [27] (see also [28]). Mundilova computed a one-parameter family of isometries that deform a planar domain into a cylindrical domain while preserving the planarity of a given curve, e.g., $\mathbf{y}^\theta: (u, v) \mapsto \alpha^\theta(u) + v(0, \cos \theta, \sin \theta)$. Then, \mathbf{x}^θ is recovered by composing \mathbf{y}^θ with a sequence of reflections about two planes, one containing the planar curve and another parallel to it, say, $\{z = 0\}$ and $\{z = \sin \theta\}$. In contrast to this geometric approach, the present analytical approach has the advantage of carrying over to other nondevelopable surfaces of translation, i.e., where the “facets” are doubly curved. Figure 3 illustrates the reach of the approach over a number of examples; details can be found in the Supplemental Material [25].

There is another purely geometric coefficient that characterizes the response of origami tessellations in bending this time. To introduce it, let \mathbf{x}^θ be a folded state, and consider an infinitesimal displacement of the form

$$\mathbf{D}: (u, v) \mapsto (x(u, v), y(u, v), z(u, v) + Eu^2/2 + Gv^2/2). \quad (11)$$

This displacement is meant to describe an effective bending displacement of \mathbf{x}^θ that induces the given normal curvatures $\kappa_1 \equiv E/I_{11}^\theta$ and $\kappa_2 \equiv G/I_{22}^\theta$. Then, the ratio of normal curvatures, namely, $\hat{\nu} \equiv -\kappa_2/\kappa_1$, mimics an “out-of-plane” Poisson's coefficient and is worthy of investigation: On the one hand, its sign indicates whether the tessellation bends into a dome or a saddle. On the other hand, its magnitude

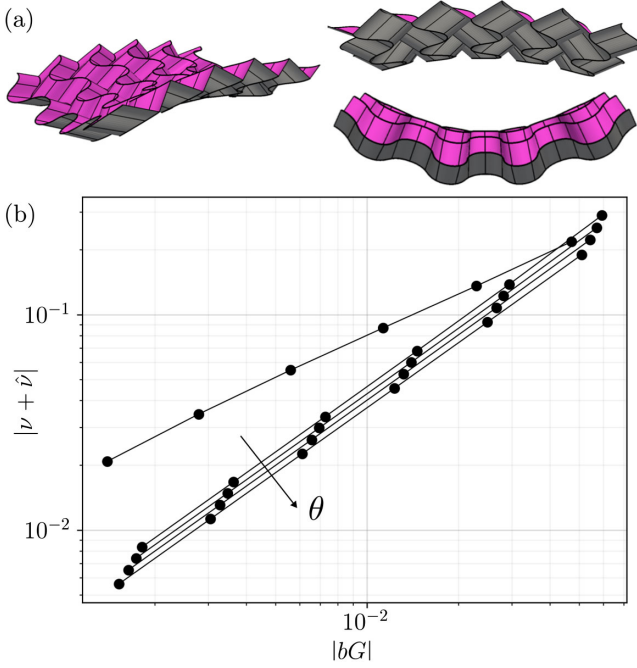


FIG. 4. Normal curvatures. (a) Infinitesimally bent state. The top (bottom) view puts forward the imposed (induced) curvature in the zigzag (curved-crease) direction. Inset: depiction of the saddle shape. (b) Identity of Poisson's coefficients. The numerical error vs normalized curvature for various folding angles θ was sampled every $\sim 5^\circ$ from $\sim 22^\circ$ to $\sim 45^\circ$; θ increases with the arrow except for the outlier which corresponds to an almost maximally folded state. (For $\theta/\Theta \sim 1$, ν changes drastically; see Fig. 2. This justifies the slower convergence rate).

quantifies the discrepancy, or lack thereof, between the curvatures in the two directions of periodicity. To find $\hat{\nu}$, one must find \mathbf{D} such that $\mathbf{x}^\theta + \mathbf{D}$ is infinitesimally isometric to \mathbf{x}^θ . For the curved-crease variant of the Miura ori under consideration, we carried numerical simulations where θ is given, G is imposed at a boundary, say, $\{u = 0\}$, \mathbf{D} is computed by propagating (infinitesimal) inextensibility constraints away from the boundary [25,29], and E is evaluated by finite differences. The infinitesimally bent state is illustrated on Fig. 4(a) and the numerical results are compiled in Fig. 4(b). These show that

$$\hat{\nu} = -\nu \quad (12)$$

up to a small error proportional to bG [30]. This identity was first discovered for the original Miura ori [6,31] and later noted for other patterns with straight creases (e.g., the “eggbox” pattern [32], the “morph” pattern [33], and “zigzag sums” [34]). A recent theoretical development shows that it holds for any periodic surface [35,36]. Identity (12) shows that the in-plane and out-of-plane responses of curved-crease origami tessellations are tied together. Although this can be a hindrance for design, e.g., free-form, purposes, it can be a major advantage for control

purposes. By imposing one curvature along a boundary, the geometry in the bulk of the tessellation's domain can be specified.

As discussed above, upon folding, the curved crease α^θ remains planar. Therefore, it is possible to produce a 3D foldable solid by stacking together copies of \mathbf{x}^θ and of its mirror image relative to $\{z = 0\}$, in an alternating fashion. Following Schenk and Guest [6], it is possible to assemble more interesting foldable solids with a self-locking property. Instead of stacking copies of \mathbf{x}^θ , consider another curved-crease origami \mathbf{y} given by

$$\begin{aligned} \mathbf{y}_u(u) &= (1, aq \cos(qu), 0), \\ \mathbf{y}_v(v) &= \begin{cases} (0, \cos \theta_o, \sin \theta_o) & \text{for } 0 \leq v < c, \\ (0, \cos \theta_o, -\sin \theta_o) & \text{for } c \leq v < 2c. \end{cases} \end{aligned} \quad (13)$$

Note that \mathbf{y} is prefolded through an initial angle θ_o equal to the initial elevation of the zigzag lines $\{u = cst\}$ of \mathbf{y} above the horizontal. Thus, it is possible to assemble \mathbf{x} and \mathbf{y} by gluing them, say, at even numbered creases $\{v = 2mb\}$ and $\{v = 2mc\}$ if the steps b and c are such that $b = c \cos \theta_o$. As \mathbf{x} folds into \mathbf{x}^θ , \mathbf{y} folds into a surface \mathbf{y}^δ defined to be isometric to \mathbf{y} in the same manner presented above, namely, with

$$\begin{aligned} \mathbf{y}_u^\delta(u) &= \left(\sqrt{1 + a^2 q^2 \cos^2(qu) \left(1 - \frac{\cos^2 \theta_o}{\cos^2(\theta_o + \delta)}\right)}, \right. \\ &\quad \left. aq \frac{\cos(qu) \cos \theta_o}{\cos(\theta_o + \delta)}, 0 \right), \\ \mathbf{y}_v(v) &= (0, \cos(\theta_o + \delta), (-1)^m \sin(\theta_o + \delta)), \end{aligned} \quad (14)$$

where the deformation parameter δ is chosen, if possible, to ensure that contact between \mathbf{x}^θ and \mathbf{y}^δ is maintained at the same even numbered creases. When the expressions for \mathbf{y}_u^δ and \mathbf{x}_u^θ are compared, it turns out that this is possible if

$$\cos(\theta_o + \delta) = \cos \theta \cos \theta_o. \quad (15)$$

By alternating copies of \mathbf{x}^θ and \mathbf{y}^δ , a foldable solid is obtained. The solid is maximally folded for $\theta = \Theta$; then, as θ decreases, it unfolds up to $\theta = 0$. At that point, $\mathbf{x}^{\theta=0} = \mathbf{x}$ is flat unfolded and brings the unfolding of the solid to a halt. This motion is illustrated in Fig. 5(a). Such solids with predetermined unfolded states provide deployable sandwich panels with curved-crease foldcores for space structures and morphing airfoil applications. Note that the maximally unfolded “locked” state can be tuned by adjusting the prefolding parameter θ_o . Note also that the Poisson's coefficients in the (x, z) and (z, y) planes can

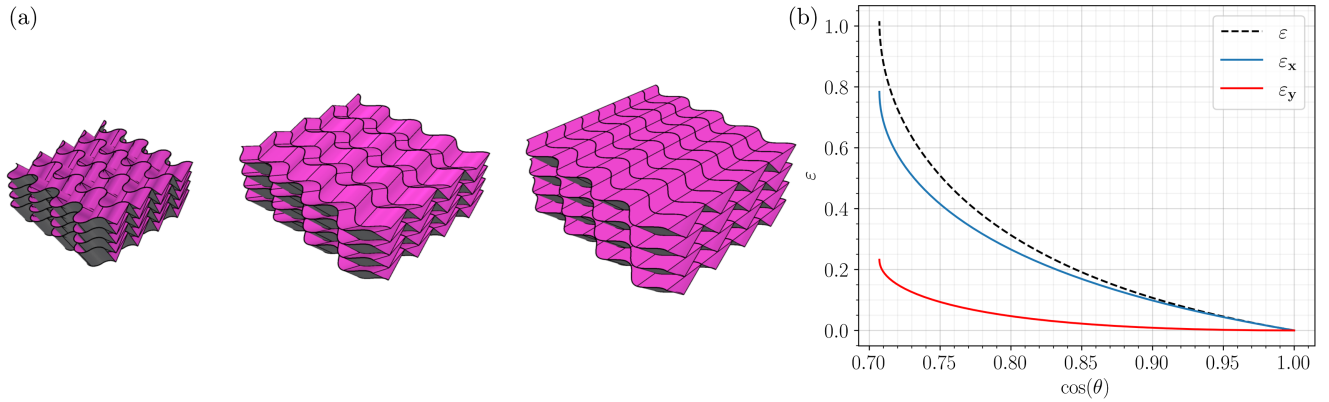


FIG. 5. Curved-crease morphing solid. (a) Left to right are maximally folded ($\theta = \Theta = \pi/4$, $\delta = \pi/12$), partially folded, and maximally unfolded ($\theta = \delta = 0$) states. Here $\theta_o = \pi/4$; other values are the same as in Fig. 1. (b) Normalized elastic energy (ε) vs elongation ($\cos \theta$).

be computed using the expressions of \mathbf{x}^θ and \mathbf{y}^δ , but this is not pursued here.

Part of the energy required to deploy the solid is due to crease folding and can be modeled as a lineal density function of dihedral angles at crease lines; this density promises to be highly nonlinear as well as material and history dependent, except in a limiting case where the creases have zero stiffness [37]. This ideal limit is adopted here and our focus shifts to the remainder of elastic energy due to bending between the creases. The fact that the deformation is isometric implies that the bending energy $\varepsilon \equiv \varepsilon(\theta)$ is a function of a single measure of curvature, e.g., the mean curvature H if the constitutive material is isotropic. Thus, up to a coefficient of bending rigidity, $\varepsilon = \varepsilon_x + \varepsilon_y$, with

$$\varepsilon_x(\theta) = \frac{1}{2} \int_0^{2\pi/q} \int_0^{2b} [H(u, v; \mathbf{x}^\theta) - H^0(u, v)]^2 dudv \quad (16)$$

being the bending energy of layer \mathbf{x} . H^0 is its mean curvature in the natural configuration and H is its mean curvature [25]. The energy ε_y is similarly defined. The profiles of ε , ε_x , and ε_y vs elongation as measured by $\cos(\theta)$ are depicted in Fig. 5(b) assuming that the natural configurations of the layers are those that occur in a maximally deployed solid. Interestingly, ε reaches the natural state with a nonzero slope; this slope is equal to the buckling load required to trigger the folding of layer \mathbf{x} out of its flat-unfolded state.

In conclusion, the presence of curved creases couples bending and folding and requires new methods for the design and analysis of deployable structures, compliant shell mechanisms and morphing metamaterials. This Letter contributes to that effort for a class of curved-crease variants of the Miura ori, as well as other developable and nondevelopable surfaces of translation. Although the methods proposed here are specific to these cases, they provide insight into the behavior of more general curved-

crease origami patterns and are a useful benchmark for the development of more universal theories and tools of numerical simulation. Analysis here was restricted to predefined deployment paths; a more general description needs to fully account for the interaction between the inextensible kinematics and the elastic energy landscape.

This work was supported by the NSF under CAREER Award No. CMMI-2045881.

*Corresponding author: nassarh@missouri.edu

- [1] G. W. Milton, *The Theory of Composites* (Cambridge University Press, Cambridge, England, 2002).
- [2] A. R. Day, K. A. Snyder, E. J. Garboczi, and M. F. Thorpe, The elastic moduli of a sheet containing circular holes, *J. Mech. Phys. Solids* **40**, 1031 (1992).
- [3] M. F. Thorpe and I. Jasiuk, New results in the theory of elasticity for two-dimensional composites, *Proc. R. Soc. A* **438**, 531 (1992).
- [4] Z. Wang, C. Luan, G. Liao, J. Liu, X. Yao, and J. Fu, Progress in auxetic mechanical metamaterials: Structures, characteristics, manufacturing methods, and applications, *Adv. Eng. Mater.* **22**, 2000312 (2020).
- [5] X. Ren, R. Das, P. Tran, T. D. Ngo, and Y. M. Xie, Auxetic metamaterials and structures: A review, *Smart Mater. Struct.* **49**, 38 (2021).
- [6] M. Schenk and S. D. Guest, Geometry of Miura-folded metamaterials, *Proc. Natl. Acad. Sci. U.S.A.* **110**, 3276 (2013).
- [7] K. A. Seffen, Compliant shell mechanisms, *Phil. Trans. R. Soc. A* **370**, 2010 (2012).
- [8] E. Demaine, M. Demaine, D. Koschitz, and T. Tachi, A review on curved creases in art, design and mathematics, *Symmetry* **26**, 145 (2015).
- [9] D. Fuchs and S. Tabachnikov, More on paperfolding, *Am. Math. Mon.* **106**, 27 (1999).
- [10] D. A. Huffman, Curvature and creases: A primer on paper, *IEEE Trans. Comput.* **C-25**, 1010 (1976).

- [11] R. D. Koschitz, Computational design with curved creases: David Huffman's approach to paperfolding, Ph. D. thesis, Massachusetts Institute of Technology, 2014.
- [12] E. Demaine, M. Demaine, V. Hart, G. N. Price, and T. Tachi, (Non)existence of pleated folds: How paper folds between creases, *Graphs Combin.* **27**, 377 (2011).
- [13] E. D. Demaine, M. L. Demaine, D. A. Huffman, D. Koschitz, and T. Tachi, Characterization of curved creases and rulings: Design and analysis of lens tessellations, *Origami*, edited by K. Miura, T. Kawasaki, T. Tachi, R. Uehara, R. J. Lang, and P. Wang-Iverson (American Mathematical Society, Providence, 2015).
- [14] E. Demaine, M. Demaine, D. Huffman, D. Koschitz, and T. Tachi, Conic crease patterns with reflecting rule lines, in *Origami 7*, edited by R. J. Lang, M. Bolitho, and Z. You (Oxford University Press, Oxford, 2018), pp. 573–590.
- [15] M. Kilian, S. Flöry, Z. Chen, N. Mitra, A. Sheffer, and H. Pottmann, Curved folding, *ACM Trans. Graph.* **27**, 1 (2008).
- [16] C. Tang, P. Bo, J. Wallner, and H. Pottmann, Interactive design of developable surfaces, *ACM Trans. Graph.* **35**, 1 (2016).
- [17] C. Jiang, K. Mundilova, F. Rist, J. Wallner, and H. Pottmann, Curve-pleated structures, *ACM Trans. Graph.* **38**, 169 (2019).
- [18] E. Demaine, K. Mundilova, and T. Tachi, *Lecture Notes on Data Engineering and Communications Technologies*, Vol. 146 (Springer International Publishing, New York, 2023), pp. 185–196.
- [19] M. A. Dias, L. H. Dudte, L. Mahadevan, and C. D. Santangelo, Geometric mechanics of curved crease origami, *Phys. Rev. Lett.* **109**, 114301 (2012).
- [20] M. A. Dias and C. D. Santangelo, The shape and mechanics of curved-fold origami structures, *Europhys. Lett.* **100**, 54005 (2012).
- [21] A. Mowitz, Finite curved creases in infinite isometric sheets, *Phys. Rev. E* **105**, 035001 (2022).
- [22] J. M. Gattas and Z. You, The behaviour of curved-crease foldcores under low-velocity impact loads, *Int. J. Solids Struct.* **53**, 80 (2015).
- [23] Y. Du, C. Song, J. Xiong, and L. Wu, Fabrication and mechanical behaviors of carbon fiber reinforced composite foldcore based on curved-crease origami, *Compos. Sci. Technol.* **174**, 94 (2019).
- [24] Y. Deng, X. Zeng, Y. Wang, J. Du, and Y. Zhang, Research on the low-velocity impact performance of composite sandwich structure with curved-crease origami foldcore, *Thin-Walled Struct.* **174**, 109106 (2022).
- [25] See Supplemental Material at <http://link.aps.org/supplemental/10.1103/PhysRevLett.132.108201> for a generalized construction, finite element analysis and mean curvature computation. The code for rendered figures and figures is available at <https://github.com/nassarh/curvedCreaseOrigami>.
- [26] T. U. Lee, Z. You, and J. M. Gattas, Elastica surface generation of curved-crease origami, *Int. J. Solids Struct.* **136–137**, 13 (2018).
- [27] K. Mundilova, On mathematical folding of curved crease origami: Sliding developables and parametrizations of folds into cylinders and cones, *Computer Aided Design* **115**, 34 (2019).
- [28] K. Mundilova and T. Wills, Proceedings of Bridges 2018: Mathematics, Art, Music, Architecture, Education, Culture, *Folding the Vesica Piscis* (Tessellations Publishing, Phoenix, 2018), pp. 535–538.
- [29] H. Nassar, A. Lebéé, and L. Monasse, Fitting surfaces with the Miura tessellation, in *Origami 7*, edited by R. J. Lang, M. Bolitho, and Z. You (Oxford University Press, New York, 2018), pp. 811–826.
- [30] The results are valid for $G \ll 1/b \sim q$. Either bending is finite and the crease pattern is refined or the crease pattern is fixed and bending is infinitesimal.
- [31] Z. Y. Wei, Z. V. Guo, L. Dudte, H. Y. Liang, and L. Mahadevan, Geometric mechanics of periodic pleated origami, *Phys. Rev. Lett.* **110**, 215501 (2013).
- [32] H. Nassar, A. Lebéé, and L. Monasse, Curvature, metric and parametrization of origami tessellations: Theory and application to the eggbox pattern, *Proc. R. Soc. A* **473**, 20160705 (2017).
- [33] P. P. Pratapa, K. Liu, and G. H. Paulino, Geometric mechanics of origami patterns exhibiting Poisson's ratio switch by breaking mountain and valley assignment, *Phys. Rev. Lett.* **122**, 155501 (2019).
- [34] H. Nassar, A. Lebéé, and E. Werner, Strain compatibility and gradient elasticity in morphing origami metamaterials, *Extreme Mech. Lett.* **53**, 101722 (2022).
- [35] H. Nassar, Isometric deformations of surfaces of translation, *Math. Mech. Complex Syst.* **12**, 1 (2023).
- [36] H. Nassar and A. Weber, Effective isometries of periodic shells, *J. Mech. Phys. Solids* 105553 (2024).
- [37] S. W. Grey, F. Scarpa, and M. Schenk, Mechanics of paper-folded origami: A cautionary tale, *Mech. Res. Commun.* **107**, 103540 (2020).